



Full length article

Flaw-insensitive fracture of a micrometer-sized brittle metallic glass

Ruitao Qu^{a,b,c}, Robert Maaß^{d,e}, Zengqian Liu^b, Dominik Tönnies^a, Lin Tian^a,
Robert O. Ritchie^f, Zhefeng Zhang^{b,*}, Cynthia A. Volkert^{a,*}

^a Institute of Materials Physics, University of Göttingen, Friedrich-Hund-Platz 1, 37077 Göttingen, Germany

^b Institute of Metal Research, Chinese Academy of Sciences, 72 Wenhua Road, Shenyang, 110016, China

^c State Key Laboratory of Solidification Processing, School of Materials Science and Engineering, Northwestern Polytechnical University, 127 West Youyi Road, Xi'an, 710072, China

^d Department of Materials Science and Engineering, University of Illinois at Urbana-Champaign, Urbana, IL 61801, USA

^e Federal Institute of Materials Research and Testing (BAM), Unter den Eichen 87, 12205 Berlin, Germany

^f Materials Sciences Division, Lawrence Berkeley National Laboratory, and Department of Materials Science and Engineering, University of California, Berkeley, CA 94720, USA



ARTICLE INFO

Article history:

Received 11 May 2021

Revised 28 July 2021

Accepted 29 July 2021

Available online 4 August 2021

Keywords:

Metallic glass

Fracture toughness

Size effect

Small-scale

ABSTRACT

Brittle materials, such as oxide glasses, are usually very sensitive to flaws, giving rise to a macroscopic fracture strength that is much lower than that predicted by theory. The same applies to metallic glasses (MGs), with the important difference that these glasses can exhibit certain plastic strain prior to catastrophic failure. Here we consider the strongest metallic alloy known, a ternary $\text{Co}_{55}\text{Ta}_{10}\text{B}_{35}$ MG. We show that this macroscopically brittle glass is flaw-insensitive at the micrometer scale. This discovery emerges when testing pre-cracked specimens with self-similar geometries, where the fracture stress does not decrease with increasing pre-crack size. The fracture toughness of this ultra-strong glassy alloy is further shown to increase with increasing sample size. Both these findings deviate from our classical understanding of fracture mechanics, and are attributed to a transition from toughness-controlled to strength-controlled fracture below a critical sample size.

© 2021 Acta Materialia Inc. Published by Elsevier Ltd. All rights reserved.

1. Introduction

Metallic glasses (MGs) are unique alloys with an amorphous structure, similar to classical oxide glasses [1]. Beyond being a metal, MGs have little in common with traditional crystalline metals. It is consequently not possible to describe mechanical failure mechanisms in MGs with classical dislocation theory that provides our fundamental framework to understand the deformation and failure of crystalline alloys. At room temperature, plastic deformation in MGs is usually localized in shear bands [2,3]. Shear banding is an inhomogeneous localized deformation process that leads to discrete plasticity in stress-strain curves if obtained in the serrated flow regime, i.e. at a temperature where the shear-band propagation rate exceeds the applied deformation rate [4,5]. It is generally accepted that the sliding stability of shear bands can be markedly improved with a reduction in sample size owing to the reduced energy release rate [6–8]. Since the critical shear offset for shear fracture has been found to be size-independent, an individual shear band can contribute more plastic strain prior

to failure in smaller sample sizes [5,9]. These features were widely reported to culminate in MGs with the increase of plastic strain at failure under various loading modes [10]. Excessive size-reduction of a MG towards the characteristic length-scale of the shear-band thickness (10–100 nm [11]) results in another size-effect where inhomogeneous strain-localization transitions to an apparent homogeneous plasticity [12,13], including the occurrence of plastic instabilities such as necking [14–16]. However, other studies on micrometer-sized MGs have reported enhanced yield strengths due to an increased resistance to shear-band initiation [17,18]. While some of these size-effects are not fully understood, there is a general consensus that fracture of brittle MGs at the bulk scale is dominated by macroscopic cleavage cracking [19], whereas a sufficient sample-size reduction can often lead to shear-band dominated ductile failure [7].

The above considerations prompt the hypothesis that MGs may exhibit size-dependent fracture properties. Indeed, Gludovatz et al. [20,21] recently performed systematic sample-size dependent fracture toughness measurements on millimeter-sized Pd-based and Zr-based MGs, finding a tendency of increasing fracture toughness for smaller samples. This is much different for traditional crystalline alloys (for example aluminum alloys) [22], but conforms well with the observation of size-dependent plasticity of MGs [10]. Given

* Corresponding authors.

E-mail addresses: zhfzhang@imr.ac.cn (Z. Zhang), volkert@ump.gwdg.de (C.A. Volkert).

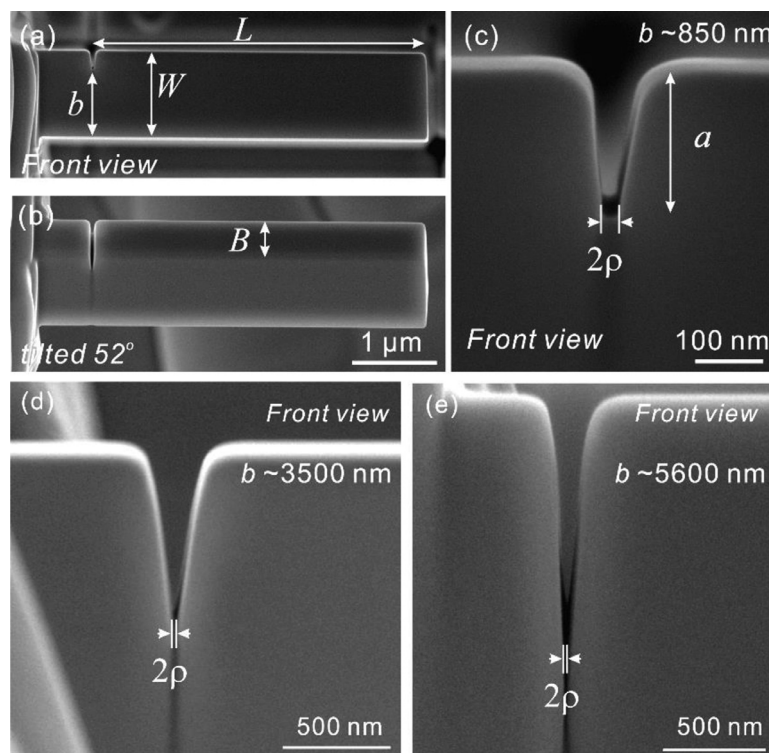


Fig. 1. External appearance and notch geometries of typical micro-fracture samples. The $\text{Co}_{55}\text{Ta}_{10}\text{B}_{35}$ MG samples shown here have different ligament sizes: (a)-(c) $b \sim 850$ nm, (d) $b \sim 3500$ nm, and (e) $b \sim 5600$ nm. B is the sample thickness, W is the sample width and ρ is the notch root radius.

that this sample-size effect on fracture occurs at the macroscopic dimensions of millimeters, the work presented here aims at uncovering the size-dependent fracture toughness of MG at the *micrometer scale*. This has been attempted in earlier studies [23–28], with the shortcoming that the toughness was usually reported for only a narrow range of sample sizes, making it an important contribution to assessing the micrometer-scale fracture toughness across a range of sizes with a statistically reliable data set.

To this end, we chose the strongest known, but macroscopically brittle, $\text{Co}_{55}\text{Ta}_{35}\text{B}_{10}$ MG, which has a yield strength of over 5 GPa [29]. This choice is motivated by the extremely small (<50 nm) plastic-zone size ahead of the crack tip, which is fundamentally associated with its low macroscopic toughness, but at the same time permits reliable fracture toughness measurements at the micrometer scale. In our study, we employed the widely used micro-fracture testing method using notched cantilever beam bending [30]. The self-similar specimens had fixed ratios of a/W and B/W (a crack length, W sample width, and B thickness, see Fig. 1(a)), similar to refs. [20,21], but of varying dimensions with W ranging from ~ 1 μm to 6.5 μm , *i.e.*, with three orders of magnitude smaller sample dimensions. These experiments demonstrate for the first time the flaw-insensitive fracture behavior of a macroscopically brittle MG at the micrometer scale.

2. Experimental

2.1. Material and sample preparation

The $\text{Co}_{55}\text{Ta}_{35}\text{B}_{10}$ (at.%) MG was prepared by an induction casting method, as described in detail in ref. [29]. 30-mm long as-cast rods were processed with a diameter of 1 mm. The amorphous structure of the material was validated by x-ray diffraction and transmission electron microscopy.

Notched cantilever beams were machined with focused ion beam (FIB) milling using a beam of 30 keV Ga^+ installed in the

FEI Nova 600 Nano Lab dual-beam scanning electron microscope (SEM). The current of ion beam was varied from 20 nA for the initial coarse milling to 0.3 nA for the final fine milling to improve efficiency and minimize FIB damage. For small samples with width smaller than 2 μm , the final fine milling current was 30 pA. To machine the notch, a much lower current of 10 pA was utilized to reduce the FIB-affected zone around the notch tip.

Fig. 1 shows the appearance of typical cantilever samples, especially the notched geometries. A nearly perfect rectangular bar with a V-shape notch can be seen, demonstrating a well-controlled sample geometry. The notches have sharp tips with radius considerably smaller than the crack length. To give a quantitative comparison, we measured the notch radius of typical cantilever samples and list them with other sample dimensions in Table 1. The results show that the notch tips are ~ 9 nm for most samples with the exception of the smallest cantilever beam, which has a slightly larger value of ~ 13 nm. The larger notch tip for the smallest sample is consistent with the somewhat higher than expected notch bending strength and toughness values measured for this sample (see below).

2.2. Micro-fracture testing

The bending test was performed with an Agilent Nano Indenter G200. The beam-end far from the notch was compressed by an indenter. The allowable thermal drift was as low as 0.05 nm/s, with the load measured using a dynamic contact module with a resolution of 1 nN. The loading rate was controlled to be constant during the test and the load and displacement values were recorded. The value of loading rate was determined to maintain a similar rate of the stress intensity K_I for all samples, *i.e.*, $dK_I/dt = 0.05$ $\text{MPa}\cdot\text{m}^{1/2}\text{s}^{-1}$. All tests were performed at room temperature, which is much lower than the glass-transition temperature (T_g) of the present Co-based MG ($T_g = 975$ K [29]), in order to minimize the influence of any temperature-dependent behavior

Table 1

Dimensions of typical cantilever beam samples. W , B and L represent the width, thickness and length of cantilever beam, respectively; a and ρ are the length and tip radius of notch.

Label	a (nm)	W (nm)	B (nm)	L (nm)	ρ (nm)	$b = W-a$ (nm)	B/W	a/W
Co-1000	204	1030	779	3900	13.2	826	0.76	0.20
Co-2000	523	2221	1677	10,670	9.8	1698	0.75	0.24
Co-3000	587	2732	2183	12,960	8.4	2145	0.80	0.21
Co-4000	811	3818	2808	13,070	8.3	3007	0.74	0.21
Co-6500	1080	6480	4357	19,740	9.1	5400	0.67	0.17

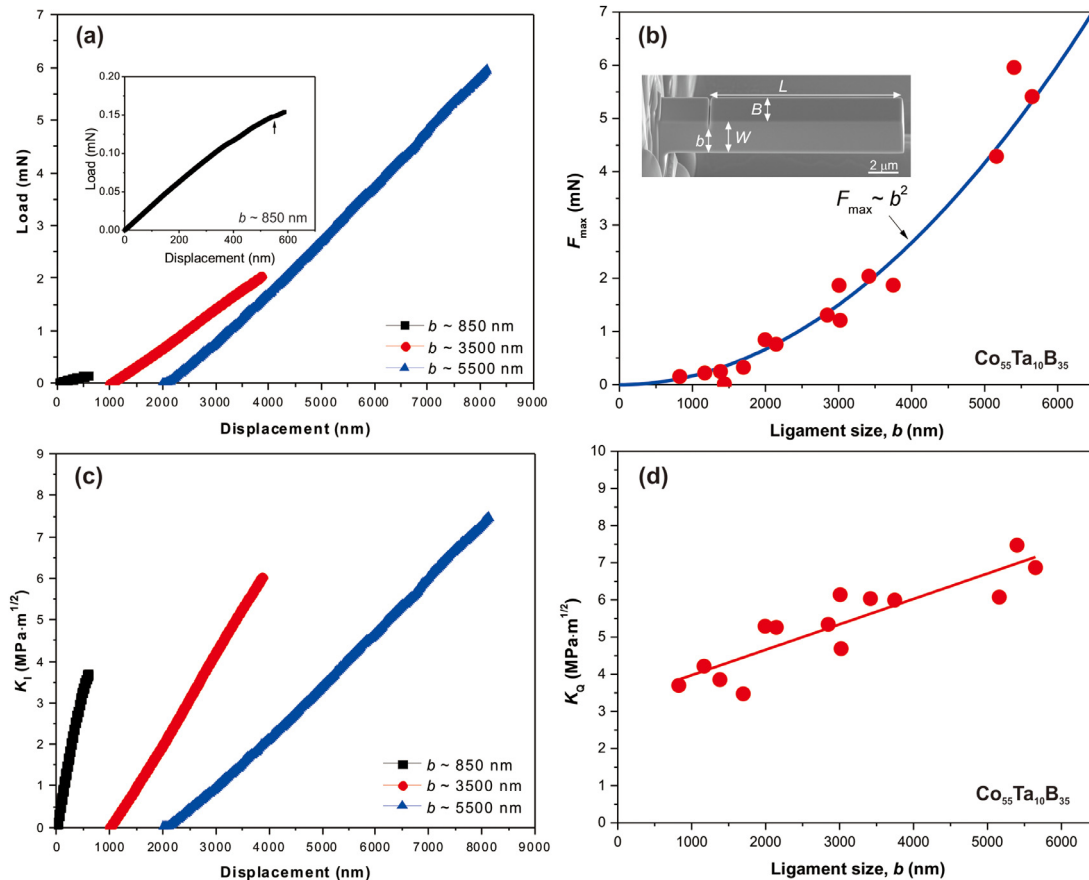


Fig. 2. Results of micro-fracture testing of $\text{Co}_{55}\text{Ta}_{10}\text{B}_{35}$ MG. (a) Typical load-displacement curves of micro-cantilever beams with different ligament size, b . Inset to (a) shows the curve of the smallest beam, where a serration was indicated. (b) Maximum load vs. ligament size. Inset to (b) displays an example of the micro-cantilever sample. (c) Typical curves of K_I vs. displacement for beams of different size. (d) Measured K_Q values as a function of b . Curves in (a) and (c) were shifted in displacement for better comparison (except those of the smallest sample). (For interpretation of the references to colour in this figure legend, the reader is referred to the web version of this article.)

and to avoid the intermediate temperature brittleness observed in some MGs [31,32].

Approximately 15 cantilever beams with different dimensions were tested and the fracture toughness results were found to be valid in terms of ASTM E399 Standard [33] for linear-elastic fracture toughness testing, as discussed in Section 4.1. For all beams, the ratio of a/W and B/W were carefully controlled to be nearly the same, with the ratio of L/b larger than 3.5. The reason for controlling the dimensions was to maintain a self-similar sample geometry, and to focus only on the effect of sample size. After the micro-fracture test, the deformation and fracture features of all samples were observed with the high-resolution SEM.

3. Results

3.1. Size effect on provisional fracture toughness

Fig. 2(a) shows representative load-displacement curves from the micrometer-scale bending experiments. Linear elastic loading is

typically observed until abrupt and final fracture sets in, at which point unstable crack propagation initiated at the notch tip ensues. For the smallest cantilever beam with a ligament size of $b \sim 850$ nm, some deviation from linear elastic loading is seen, which is due to localized plasticity at the relatively larger notch-tip radius ($\rho \sim 13$ nm) than for the large cantilevers ($\rho \sim 9$ nm, see Table 1). Larger cantilever beams appear to be stiffer, but due to the difficulty in accurately measuring the displacement at these scales, we will focus on the fracture loads that increase with ligament size. Plotting the maximum load (F_{\max}) of each sample as a function of the ligament size b in Fig. 2(b), we find that the data can be well fitted with a scaling relationship as $F_{\max} \propto b^2$. Subsequently, we computed the stress-intensity factor (K_I) for the notched cantilever beam via [34]:

$$K_I = \frac{FL}{BW^{3/2}} f\left(\frac{a}{W}\right), \quad (1)$$

where F is the load and L is beam length (from notch to loading point). $f(a/W)$ is the geometry factor that needs to be derived

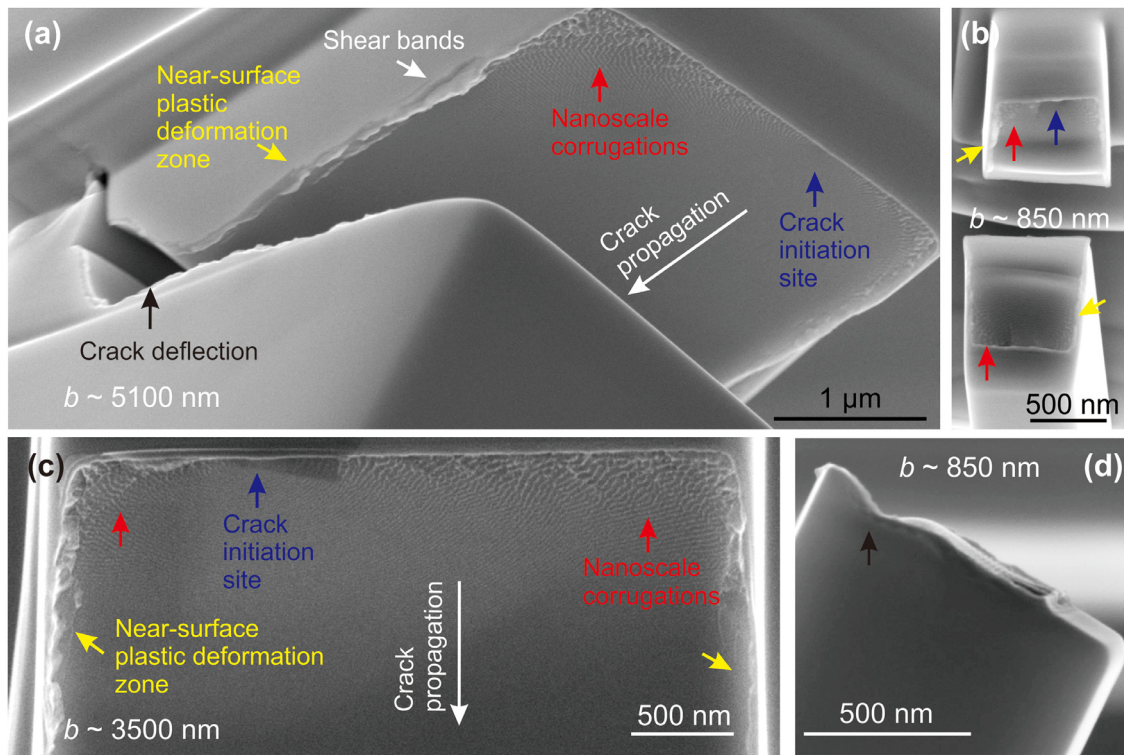


Fig. 3. Fracture morphologies of micrometer-sized $\text{Co}_{55}\text{Ta}_{10}\text{B}_{35}$ MG. (a)–(c) Fracture surface morphologies of samples with ligament size of ~ 5100 nm, ~ 850 nm and ~ 3500 nm, respectively. Crack initiation site, nanoscale corrugations and near-surface plastic deformation zone are indicated by blue, red and yellow arrows, respectively. (d) Side-view of the fracture surface of a sample with $b \sim 850$ nm. (For interpretation of the references to colour in this figure legend, the reader is referred to the web version of this article.)

numerically. For the present beams with $B/W \sim 0.8$, Iqbal et al. [34] determined the expression $f(a/W)$ with finite element modeling to be given by:

$$f\left(\frac{a}{W}\right) = 77.608\left(\frac{a}{W}\right)^3 - 48.422\left(\frac{a}{W}\right)^2 + 24.184\left(\frac{a}{W}\right) + 1.52. \quad (2)$$

Based on Eq. (1), the real-time K_I was calculated and plotted as a function of the displacement, as shown in Fig. 2(c). Since the measurements do not indicate any significant plastic deformation, K_I represents the onset of the fracture instability and is therefore linked to the maximum applied load. Hence this value of K_I can be equated with the well-defined provisional fracture toughness K_Q , i.e.,

$$K_Q = \frac{F_{\max}L}{BW^{3/2}} \cdot f\left(\frac{a}{W}\right). \quad (3)$$

Conducted across 15 samples with different dimensions, this analysis reveals the surprising result that smaller samples have lower K_Q values, as can be seen in Fig. 2(d). Thus, larger MG samples are tougher, which stands in stark contrast to the reported increasing trend of toughness [20,21] and ductility [10] upon sample-size reduction in larger (millimeter-sized and above) samples, but is consistent with the previous micro-cantilever toughness measurements on a Zr-based MG [25]. Therefore, this gives rise to an important scientific question: are the smaller samples tougher or not?

3.2. Deformation and fracture features

The deformation features and fracture surface-morphologies of typical cantilever beams are displayed in Fig. 3. For all samples, al-

though their sizes are different, the deformation and fracture surfaces are similar. We can identify three main common features. Firstly, the majority of the fracture surface of each sample is covered by nanoscale corrugations that are constituted by numerous nano-ridges, similar to the fracture morphology of bulk samples of brittle MGs [19,35]. Secondly, the crack initiation site is located in the interior of the sample and ahead of the notch tip, where strong stress triaxiality is generated to facilitate cavitation [36]. This is consistent with the previous findings in bulk samples of an embrittled MG [37], suggesting a similar brittle fracture mechanism. Thirdly, plastic deformation zones of shear bands were observed in front of the notch tip on the side surfaces of all samples (Fig. 3(a)), similar to those observed in ductile MGs tested in bulk samples [20,38]. However, the deformation zones here observed in the small-scale brittle $\text{Co}_{55}\text{Ta}_{10}\text{B}_{35}$ MG samples have strip-like shapes with very limited number of shear bands.

From the high-resolution electron microscopy observations on the sample surfaces (Fig. 4) we can see that the plastic deformation in both large and small samples is localized in a narrow, strip-like zone, formed by a few shear bands with directions nearly parallel to the crack plane. This appearance of deformation zone is markedly different from the plastic zone of ductile MGs [21,32,38], where primary shear bands with shear angles approaching 45° with respect to the crack plane tend to form in a much wider plastic zone. The strip-like plastic deformation zone has a maximum width of ~ 144 nm for the large sample with $b > 5 \mu\text{m}$ and ~ 54 nm for the smallest one with $b \sim 850$ nm. These length-scales are consistent with the toughness values of the samples, i.e., tougher samples have larger plastic zones, but their dimensions are negligible compared to the sample dimensions such as the ligament size or sample thickness. This is also in perfect agreement with the lack of plastic events in the load-deflection curves. However, these val-

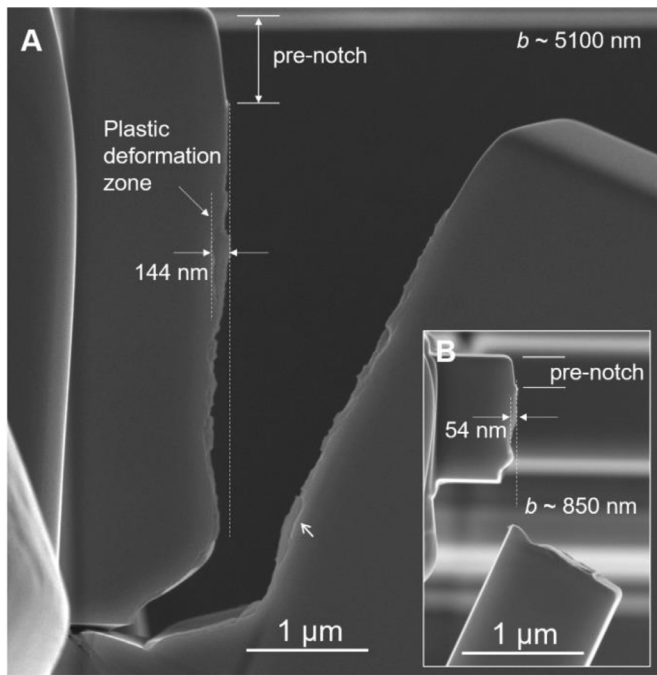


Fig. 4. Strip-like plastic deformation zone on the sample surface due to the shear lip formation for two samples with different sizes. The ligament sizes for (a) and (b) are ~ 5100 nm and ~ 850 nm, respectively.

ues are different from the plastic-zone size defined by continuum fracture mechanics [39], which defines the plastic-zone size as the length of the plastic zone along the cracking direction before unstable fracture (see further discussion in Section 4.1). The strip-like zone is more likely the shear lip region formed in the fracture process, rather than a plastic zone ahead of the crack tip before the unstable crack propagation. This can be confirmed by the fracture surface observations. As shown in Figs. 3 and 5, at the two edges of the fracture surface, narrow regions of shear lips can be easily seen. These align well with the strip-like plastic deformation zones on the sample surfaces.

The fracture surface is covered mostly by nanoscale corrugations with a decreasing wavelength as a function of increasing distance from the notch tip, implying that fast crack propagation initiates from a site close to the notch tip, as indicated by the white arrows in Fig. 5. It is suggested that the peak stress triaxiality ahead of a crack is located ~ 2 CTODs from the crack tip [40], where CTOD is the crack-tip opening displacement. The CTOD can be estimated as [39]: $CTOD = 4K_I^2 / (\pi E \sigma_y)$, where E is Young's modulus. Substituting $K_I = K_Q$, $\sigma_y = 7.5 \pm 0.7$ GPa and $E = 240$ GPa into above equation, we estimated the CTOD for the largest beam to be ~ 30 nm. Consequently, the crack initiation site is expected to be located in the vicinity of ~ 60 nm ahead from the notch tip, which is consistent with the experimental results shown in Fig. 5, implying local stress-controlled brittle fracture [37,40].

The fracture surface features in the present Co-based MG micro-fracture samples are markedly different from the fracture surface morphologies in ductile MGs [41], where a notch blunting zone usually forms close to the notch tip. The notch blunting zone is typically followed by a Taylor meniscus instability zone [41], caused by unstable fracture along shear bands of the MGs. Both the notch blunting and the Taylor meniscus instability zones are evidence for the shear banding deformation in front of the notch. However, in the present Co-based MG micro-scale notched cantilever specimens, no obvious evidence of shear banding activity ahead of the notch tip can be observed.

We further observe that crack deflection occurs in the final stage of fracture (Fig. 4(a)), which we attribute to the complexity of the stress state at the point when the remaining ligament becomes much smaller than the sample width (W). The similar fracture morphologies strongly underline identical deformation and fracture mechanisms across all sample sizes.

3.3. Size effect on notch bending strength

For the current notch bending tests, we estimate the real-time notch bending stress, σ_{nbs} , i.e., the maximum of nominal tensile stress at the notch tip, as,

$$\sigma_{nbs} = \frac{6FL}{B(W-a)^2}, \quad (4)$$

where F is the real-time load. Accordingly, some typical curves of notch bending stress vs. displacement of several micro-fracture samples are plotted in Fig. 6. The nominal bending stress increases with increasing deformation prior to fracture which happens catastrophically without indications of any obvious plasticity. Although the sample dimensions of the present micro-cantilevers vary over a wide range, the notch bending stresses at the onset of fracture, i.e., the notch bending strength σ_{nb} , are very similar, in contrast to the measured toughness values (Fig. 2(d)).

To illustrate this size-independence of the notch bending strength more clearly, we plotted the values of σ_{nb} for our micrometer-sized Co-based MG as a function of sample width (W) in Fig. 7(a). No obvious size effect was observed for σ_{nb} at the studied length-scale, although the data show some scatter as expected [42]. Therefore, when comparing this result with the measured toughness values (Fig. 2(d)), we can conclude that the occurrence of fracture in the micrometer-sized Co-based MG is dominated by a critical stress rather than the stress-intensity factor – that is, the fracture is strength-controlled but not toughness-controlled at these small size-scales.

Furthermore, by combing Eqs. (3) and (4), one finds,

$$K_Q = \sigma_{nb} \sqrt{W} \cdot g\left(\frac{a}{W}\right), \quad (5)$$

where $g\left(\frac{a}{W}\right) = \frac{1}{6} \left(1 - \frac{a}{W}\right)^2 f\left(\frac{a}{W}\right)$, is a geometry factor. Plotting $K_Q/g(a/W)$ as a function of the sample width, as shown in Fig. 7(b), it is apparent that Eq. (5) with $\sigma_{nb} = 5.4$ GPa can excellently fit the measured toughness data in the different samples. This agreement suggests that the size-dependence of K_Q results from the size-independence of the notch bending strength and that it is not associated with a change of any intrinsic deformation mechanism. From the electron microscopy observations, indeed we cannot discern any differences in either the deformation and fracture features between the different-sized samples.

4. Discussion

4.1. Continuum estimation of plastic zone size

A plastic zone will form ahead of a crack tip. For a valid fracture toughness measurement, the plastic zone should be far smaller than the crack length, the ligament width and the sample thickness, in order to satisfy the conditions in terms of small-scale yielding and plane strain [33,39]. In Section 3.2, we showed the experimental observations of the strip-like plastic deformation zone on the sample surfaces with the maximum width of ~ 54 – 144 nm for samples with different sizes. The fracture surface features suggest that the strip-like plastic deformation zone may not be the plastic zone ahead of crack tip defined by continuum fracture mechanics [39], and the latter may be smaller. In the following, we here estimate the plastic-zone size based on the continuum mechanics solution and discuss the validity of the toughness data.

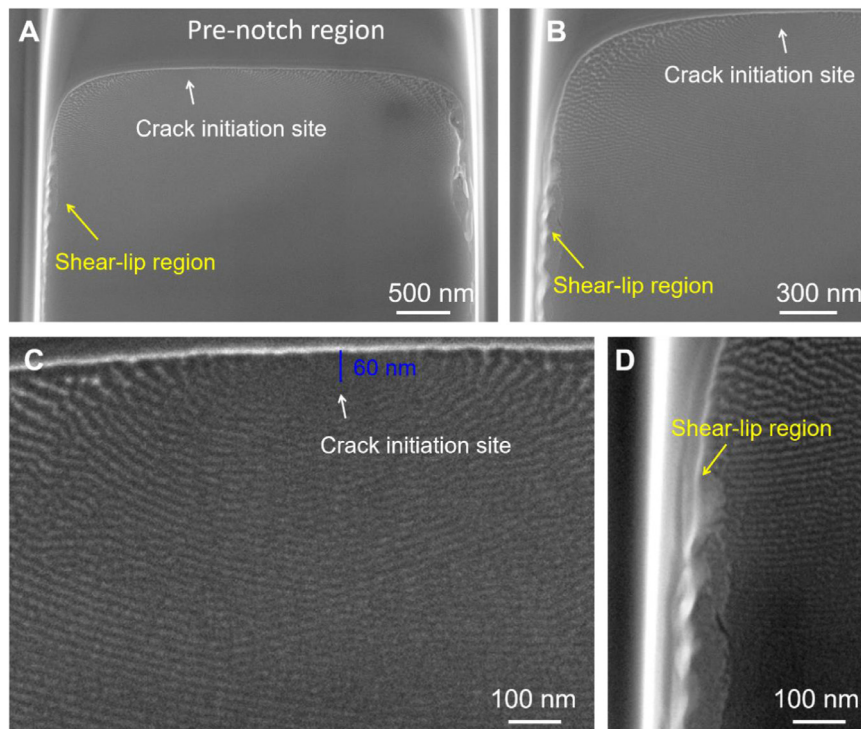


Fig. 5. Fracture surface morphologies of the largest cantilever beam with ligament size $b \sim 5600$ nm. Crack initiation site, nanoscale corrugations and shear lip regions can be clearly seen.

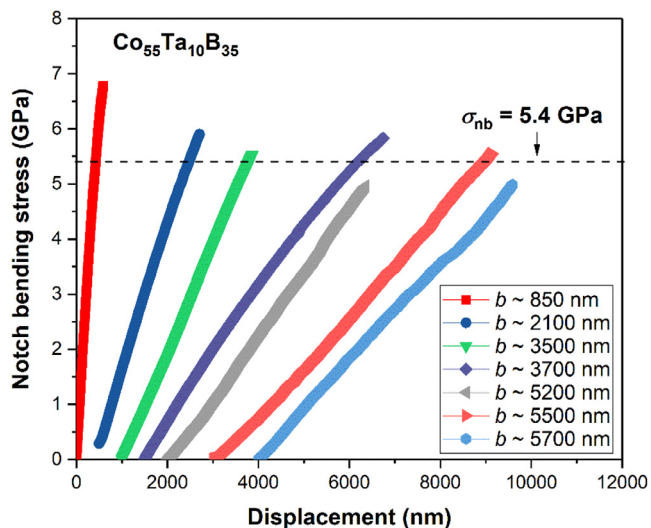


Fig. 6. Notch bending stress-displacement curves. The curves of typical microfracture samples with different ligament sizes are shown here. The average notch bending strength (σ_{nb}), i.e., the notch bending stress at fracture, is indicated for comparison. Curves, except for that of the smallest sample, are horizontally shifted in displacement for clarity.

With the assumption that the boundary between elastic and plastic deformation occurs when the stress in the tensile direction equals the yield strength, the plastic-zone size, r_y , under plane-stress condition directly ahead of the crack tip can be approximated by [39]:

$$r_y = \frac{1}{2\pi} \left(\frac{K_I}{\sigma_y} \right)^2, \quad (6)$$

where σ_y is the yield strength of the material and K_I is the mode-I stress-intensity factor. In plane strain, yielding is suppressed by

Table 2

Toughness, notch bending stress and estimated plastic-zone sizes of all the testing specimens. Here K_Q , σ_{nb} , r_y and r_{y1} are toughness, notch bending stress, plane-stress plastic zone size and plane-strain plastic zone size, respectively. The plastic zone sizes were estimated from continuum mechanics. The ratios of crack length (a), ligament size ($b = W-a$), out-of-plane sample thickness (B) over plane-stress plastic zone size (r_y) are also listed.

No.	b nm	K_Q MPa·m ^{1/2}	σ_{nb} GPa	r_y nm	r_{y1} nm	a/r_y	b/r_y	B/r_y
1	826	3.70	6.78	39	13	5.3	21.3	20.1
2	1170	4.21	5.99	50	17	15.0	23.3	38.6
3	1382	3.85	5.24	42	14	11.5	32.9	35.1
4	1698	3.47	4.32	34	11	15.3	49.7	49.1
5	1915	5.09	5.65	73	24	17.1	26.1	30.6
6	1993	5.29	6.02	79	26	8.4	25.2	34.5
7	2145	5.26	5.90	78	26	7.5	27.4	27.9
8	2846	5.34	5.15	81	27	10.4	35.3	30.4
9	3007	6.14	5.83	107	36	7.6	28.2	26.3
10	3021	4.69	4.36	62	21	15.3	48.5	52.6
11	3416	6.03	5.53	103	34	7.4	33.1	32.6
12	3746	5.99	5.82	102	34	5.1	36.8	24.4
13	5160	6.08	4.96	105	35	7.2	49.3	33.2
14	5400	7.47	5.56	158	53	6.8	34.2	27.6
15	5650	6.87	5.02	134	45	8.2	42.3	30.0

the triaxial stress state, and thus the extent of the plastic zone directly ahead of the crack tip can be considered to be smaller and is typically given by [39]:

$$r_{y1} = \frac{1}{6\pi} \left(\frac{K_I}{\sigma_y} \right)^2. \quad (7)$$

By substituting $K_I = K_Q$ into Eqs. (6)-(7), we estimated the plastic-zone sizes at fracture for all samples and listed the values in Table 2. Here the yield strength value of $\sigma_y = 7.5$ GPa was used, which is higher than the yield strength of the Co-based MG measured from bulk samples (~6 GPa) [7]. The reason for using this higher strength value is because the plastic deformation ahead of the notch tip in the current micrometer sized sample is expected

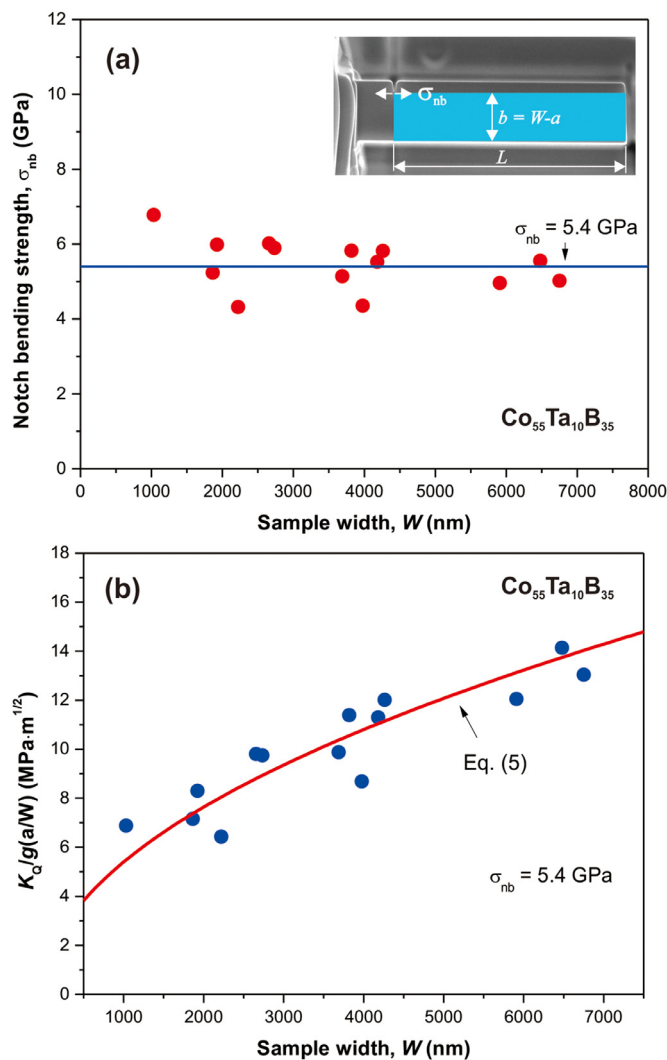


Fig. 7. Strength and toughness of samples with different sizes. (a) Notch bending strength (σ_{nb}) and (b) $K_Q/g(a/W)$ as a function of sample width. The blue part in the inset to (a) displays the reduced beam or the ligament with only the net-section area used for calculating the maximum nominal tensile stress at the notch tip. The red curve in (b) was plotted according to Eq. (5). (For interpretation of the references to colour in this figure legend, the reader is referred to the web version of this article.)

to occur in a considerably smaller volume. If we use the yield strength of ~ 6 GPa for bulk sample with the toughness measured with the largest micro-fracture sample, we conservatively estimate the plastic-zone size to be $r_y \sim 200$ nm. However, to obtain a more reasonable estimate of the plastic-zone size, we should use the yield strength corresponding to the small volume, with a length scale of ~ 200 nm, which would give a yield strength value of $\sigma_y = 7.5$ GPa, *i.e.*, as measured [7] using micropillars with diameters close to 200 nm on the same MG material.

We can see that the plane-stress plastic-zone size estimated by this continuum approach, r_y , is significantly smaller than the out-of-plane sample thickness B with $B/r_y > 20$, demonstrating that *all the samples are under plane-strain conditions*. Moreover, the estimated r_y is also much smaller than the ligament size $b (=W-a)$ with $b/r_y > 20$, and smaller than crack length with $a/r_{y0} > 5$ for all the samples. Although the crack lengths (a) for some samples are not an order of magnitude higher than r_y , there are still 6 samples fully satisfying the condition for *small-scale yielding*. To see if the small-scale yielding condition affects the conclusion of the present findings, we used the data of the above 6 samples with $a/r_{y0} >$

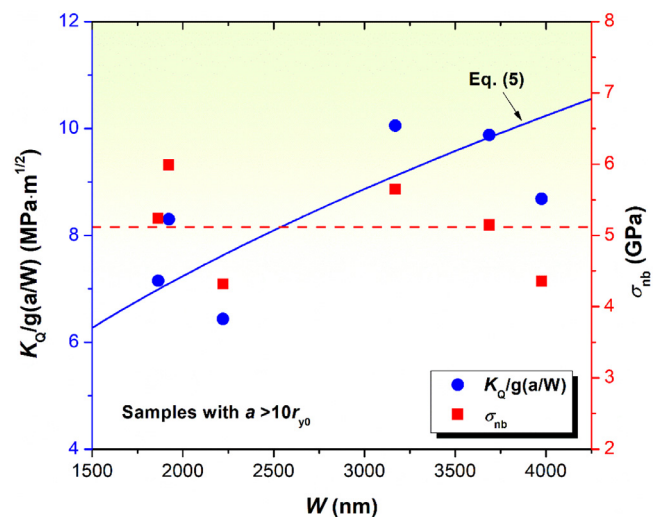


Fig. 8. Notch bending strength (σ_{nb}) and $K_Q/g(a/W)$ as functions of sample width for samples with $a > 10r_{y0}$. The solid curve is plotted according to Eq. (5), while the dashed curve shows the average notch bending strength of the samples with $a > 10r_{y0}$.

10 and plotted the notch bending strength σ_{nb} , and $K_Q/g(a/W)$ as functions of sample width W in Fig. 8. We found that with the increase of sample width, the trend still exists in terms of increasing toughness and nearly constant strength with the relation between $K_Q/g(a/W)$ and W well fitted by Eq. (5), as shown in Fig. 8.

4.2. Strength-controlled fracture vs. toughness-controlled fracture

For a brittle plate sample that contains a central through-thickness crack with length of $2a$ and that is subjected to tensile loading with the loading axis normal to the crack plane, *i.e.*, a mode-I crack, the fracture strength of the pre-cracked sample is usually controlled by fracture toughness K_{Ic} , *i.e.* [39],

$$\sigma_f = K_{Ic}/Y\sqrt{\pi a}, \quad (8)$$

where Y is a geometry factor of the crack system which is a function of a/W . The nominal fracture strength, defined as the maximum load divided by the net section area at the crack position, can be expressed as,

$$\sigma_{nf} = \frac{1}{1-a/W}\sigma_f = K_{Ic}/Y'\sqrt{\pi a}, \quad (9)$$

where $Y' = Y(1-a/W)$ is another geometry factor.

Since the plane-strain fracture toughness K_{Ic} of brittle materials is constant and independent of sample size (above the required sample thickness for plane-strain conditions to prevail), Eq. (9) suggests a decreasing nominal fracture strength with increasing crack length. For self-similar samples with fixed a/W , σ_{nf} should therefore be lower in larger samples. However, the present results show that the notch bending strength σ_{nb} , equivalent with σ_{nf} , does not drop with the increase of sample size. Indeed, the present Co-based MG demonstrates a *flaw-insensitive behavior* at the micrometer scale, although it is quite brittle and flaw-sensitive in its bulk form.

Eq. (9) predicts an infinitely large strength value as the crack size approaches zero, which is clearly not physically possible. There must be a critical crack size a_c , or a critical sample size W_c for such self-similar samples, below which Eq. (9) no longer holds. For pre-cracked samples with a size smaller than W_c or with a crack size smaller than a_c , the critical stress to cause failure based on Eq. (9) will be higher than σ_0 , the tensile fracture strength of material. At this limit the fracture will be controlled by the

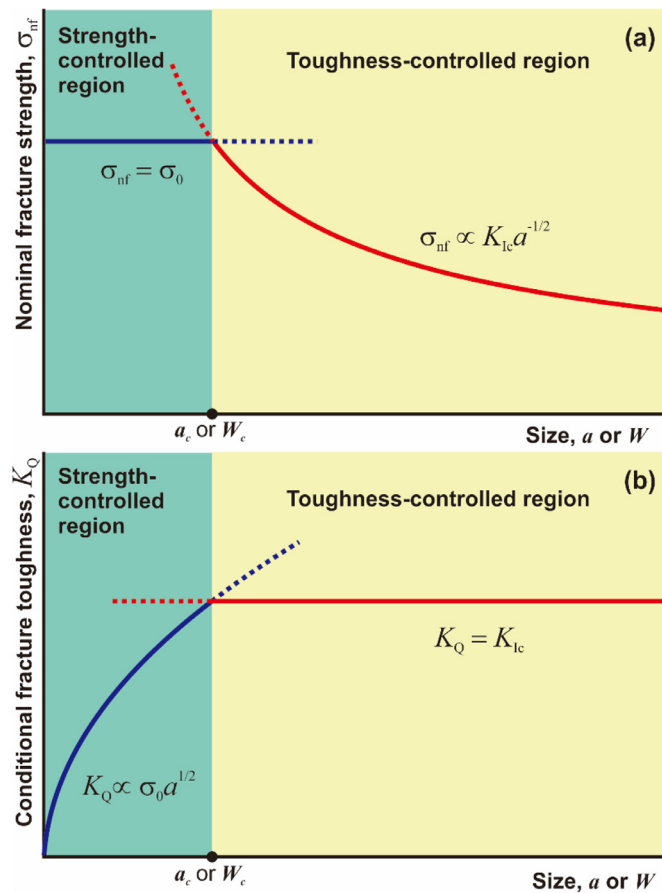


Fig. 9. Illustrations of size effect on strength and toughness of brittle MGs. (a) Size effect on the nominal fracture strength; (b) size effect on the conditional fracture toughness. Note here the samples have self-similar geometries (where a/W is fixed).

strength but not the fracture toughness K_{Ic} . Therefore, the conditional fracture toughness values measured with small-scale samples should scale with \sqrt{a} or \sqrt{W} for self-similar samples, as schematically illustrated in Fig. 9. These predictions agree well with the present results (Fig. 7), rationalizing the finding that fracture of the micrometer-sized specimens is strength-controlled rather than fracture-toughness-controlled.

The above described findings are not limited to the current Co-based MG, but are consistent with the micro-mechanical testing results of Kontis et al. [27] on CoTaB MG thin films with different compositions which demonstrated that the flexural strength and fracture toughness do not follow the general trade-off relationship [43]. Instead, these thin film experiments revealed a higher toughness for higher strength. On the other hand, for ductile MGs, the toughness data measured from micrometer-sized samples have been found to be much lower than that measured with macroscopic-sized samples [24,26,28]. For instance, K_Q values measured with microscale samples of Pd-based [28], Zr-based [24] and Cu-based MGs [26] all demonstrate a typical range of ~ 2 to $5 \text{ MPa}\cdot\text{m}^{1/2}$, which is an order of magnitude lower than in bulk samples [44,45]. However, toughness values higher than the above small-scale ductile MGs have been measured for brittle but stronger MGs, such as Co- and Fe-based MGs (e.g., in refs. [23,26,27] and the present results). Based on our understanding, such results are only physically justified if fracture at the micrometer-scale is strength-controlled.

The critical sample size W_c in notched cantilever beam bending can be calculated by substituting K_Q in Eq. (5) with K_c , which is the notch-toughness value measured using large enough samples

with self-similar geometries:

$$W_c = \left(\frac{K_c}{g(a/W)\sigma_{nb}} \right)^2. \quad (10)$$

For the present Co-based MG, we have also measured the notch-toughness value using a single edge-notched bend test sample with a diameter of $\sim 1 \text{ mm}$ (described in the Supplementary Materials). The measured notch-toughness K_c for $\text{Co}_{55}\text{Ta}_{35}\text{B}_{10}$ MG is $\sim 7 \text{ MPa}\cdot\text{m}^{1/2}$. Moreover, by substituting the values of (a/W) for each cantilever into Eq. (2) and $g(a/W) = \frac{1}{6}(1 - \frac{a}{W})^2 f(\frac{a}{W})$, we get $g(a/W) = 0.54$; and the notch bending strength $\sigma_{nb} = 5.4 \text{ GPa}$ (see Fig. 8(b)). Thus, the critical sample size for the occurrence of strength-controlled fracture behavior of notched cantilever beams is estimated to be $W_c \sim 6 \mu\text{m}$. This estimate suggests that the fracture of the alloy will be controlled by strength only when the sample size is smaller than W_c . For more ductile MGs, such as Zr-based or Pd-based alloys, the critical sample size will be much larger compared to the brittle MGs. For instance, using K_{Ic} of $30 \text{ MPa}\cdot\text{m}^{1/2}$ and flexural strength of 3 GPa which are typical for Zr-based MGs [35,45,46], from Eq. (10) the critical sample size for strength-controlled fracture W_c will be $\sim 343 \mu\text{m}$. Although further experimental verification is needed, the above estimate suggests an order of magnitude larger critical sample size for the Zr-based MGs than that for the Co-based MG, which implies that the transition between strength-controlled fracture and toughness-controlled fracture will be shifted to considerably larger length scales for more ductile alloys. However, it is worth pointing out that W_c in ductile MGs is usually much smaller than the critical sample size for small-scale yielding, plane-strain conditions, meaning that W_c defines only a necessary and not sufficient condition for fracture toughness testing in ductile MGs. Besides, the above discussion for W_c is limited to the fracture toughness defined by linear elastic fracture mechanics. For ductile materials where plastic deformation dominates energy consumption during fracturing, the elastic-plastic fracture mechanics-based methods should be considered for the measurement of toughness.

Finally, we note that the size-dependent fracture toughness at the micrometer scale in MGs is fundamentally different from most previous reports, where increased toughness values are ascribed to thicker samples, because of the fact that the toughness was not always measured under plane-strain conditions [47,48]. Here we test geometrically self-similar samples where conditions largely pertain to plane strain (except very close to the sample surface). This is very much supported by the fracture surface morphologies (Figs. 3 and 5) that exhibit nanoscale corrugations from fracture due to normal stress, whereas only the very-near surface regions exhibit evidence for the plane-stress shear lips.

5. Conclusions

By performing micro-fracture tests under small-scale yielding, plane-strain conditions, we found that the size of microscale samples strongly affects the measured fracture toughness of brittle MGs, but not in the expected fashion as for macroscale samples. The fracture strength of notched cantilever beams of the $\text{Co}_{55}\text{Ta}_{10}\text{B}_{35}$ MG was found to be independent of the sample size or pre-crack size, demonstrating a flaw-insensitive behavior. This is shown to result from a strength-controlled fracture mode, which is markedly different from the toughness-controlled fracture of macroscale samples, but is consistent with the previous notions for the fatigue failure of materials with short cracks [49] and the flaw insensitivity of natural materials at the nanoscale [50]. In addition to the fundamentally different flaw-insensitive and strength-controlled fracture at the microscale, these results demonstrate that reliability and mechanical design at the micrometer-scale with

MGs requires a different approach than conventionally used for bulk systems. Specifically, the exceptionally high strength of MGs sets the design limit irrespective of flaw size, thereby strongly outperforming conventional crystalline alloys.

Declaration of Competing Interest

We declare that we have no known financial interests or personal relationships that could inappropriately influence the work reported in this paper.

Acknowledgements

We thank Volker Radisch for technical support of the experiments. This work was financially supported by the National Natural Science Foundation of China (NSFC) under Grant nos. 51771205, and the Alexander von Humboldt (AvH) Foundation. R.O.R. was supported by the U.S. Department of Energy, Office of Science, Office of Basic Energy Sciences, Materials Sciences and Engineering Division, under contract no. DE-AC02-05CH11231. R.M. is grateful for startup funds provided by the Department of Materials Science and Engineering at UIUC. Z.F.Z. and Z.L. were supported by the KC Wong Education Foundation (GJTD-2020-09).

Supplementary materials

Supplementary material associated with this article can be found, in the online version, at doi:10.1016/j.actamat.2021.117219.

References

- [1] C.J. Byrne, M. Eldrup, Bulk Metallic Glasses, *Science* 321 (5888) (2008) 502–503.
- [2] C.A. Schuh, T.C. Hufnagel, U. Ramamurty, Mechanical behavior of amorphous alloys, *Acta Mater.* 55 (2007) 4067–4109.
- [3] A.L. Greer, Y.Q. Cheng, E. Ma, Shear bands in metallic glasses, *Mater. Sci. Eng. R* 74 (4) (2013) 71–132.
- [4] R. Maaß, J.F. Löffler, Shear-band dynamics in metallic glasses, *Adv. Funct. Mater.* 55 (2015) 2353–2368.
- [5] R.T. Qu, Z.Q. Liu, G. Wang, Z.F. Zhang, Progressive shear band propagation in metallic glasses under compression, *Acta Mater.* 91 (2015) 19–33.
- [6] R.T. Qu, S.G. Wang, X.D. Wang, S.J. Wu, Z.F. Zhang, Shear band fracture in metallic glass: sample size effect, *Mater. Sci. Eng. A* 739 (2019) 377–382.
- [7] R. Qu, D. Tonnie, L. Tian, Z. Liu, Z. Zhang, C.A. Volkert, Size-dependent failure of the strongest bulk metallic glass, *Acta Mater.* 178 (2019) 249–262.
- [8] Z. Han, W.F. Wu, Y. Li, Y.J. Wei, H.J. Gao, An instability index of shear band for plasticity in metallic glasses, *Acta Mater.* 57 (5) (2009) 1367–1372.
- [9] F.F. Wu, Z.F. Zhang, S.X. Mao, Size-dependent shear fracture and global tensile plasticity of metallic glasses, *Acta Mater.* 57 (1) (2009) 257–266.
- [10] J.R. Greer, J.T.M. De Hosson, Plasticity in small-sized metallic systems: intrinsic versus extrinsic size effect, *Prog. Mater. Sci.* 56 (6) (2011) 654–724.
- [11] C. Liu, V. Roddatis, P. Kenesei, R. Maass, Shear-band thickness and shear-band cavities in a Zr-based metallic glass, *Acta Mater.* 140 (2017) 206–216.
- [12] C.A. Volkert, A. Donohue, F. Spaepen, Effect of sample size on deformation in amorphous metals, *J. Appl. Phys.* 103 (2008) 083539.
- [13] D. Tönnies, R. Maaß, C.A. Volkert, Room temperature homogeneous ductility of micrometer-sized metallic glass, *Adv. Mater.* 26 (32) (2014) 5715–5721.
- [14] R.L. Narayan, L. Tian, D. Zhang, M. Dao, Z.-W. Shan, K.J. Hsia, Effects of notches on the deformation behavior of submicron sized metallic glasses: insights from in situ experiments, *Acta Mater.* 154 (2018) 172–181.
- [15] L. Tian, Z.-W. Shan, E. Ma, Ductile necking behavior of nanoscale metallic glasses under uniaxial tension at room temperature, *Acta Mater.* 61 (13) (2013) 4823–4830.
- [16] J. Yi, W.H. Wang, J.J. Lewandowski, Sample size and preparation effects on the tensile ductility of Pd-based metallic glass nanowires, *Acta Mater.* 87 (2015) 1–7.
- [17] C.C. Wang, J. Ding, Y.Q. Cheng, J.C. Wan, L. Tian, J. Sun, Z.W. Shan, J. Li, E. Ma, Sample size matters for Al₈₈Fe₇Gd₅ metallic glass: smaller is stronger, *Acta Mater.* 60 (13–14) (2012) 5370–5379.
- [18] L. Tian, Y.-Q. Cheng, Z.-W. Shan, J. Li, C.-C. Wang, X.-D. Han, J. Sun, E. Ma, Approaching the ideal elastic limit of metallic glasses, *Nat. Commun.* 3 (2012) 609.
- [19] G. Wang, D.Q. Zhao, H.Y. Bai, M.X. Pan, A.L. Xia, B.S. Han, X.K. Xi, Y. Wu, W.H. Wang, Nanoscale periodic morphologies on the fracture surface of brittle metallic glasses, *Phys. Rev. Lett.* 98 (23) (2007) 235501–235504.
- [20] B. Gludovatz, S.E. Naleway, R.O. Ritchie, J.J. Kruzic, Size-dependent fracture toughness of bulk metallic glasses, *Acta Mater.* 70 (2014) 198–207.
- [21] B. Gludovatz, D. Granata, K.V.S. Thurston, J.F. Löffler, R.O. Ritchie, On the understanding of the effects of sample size on the variability in fracture toughness of bulk metallic glasses, *Acta Mater.* 126 (2017) 494–506.
- [22] J.A. Joyce, R.L. Tregoning, Development of consistent size criteria for ASTM combined fracture mechanics standards, in: K.L. Jerina, P.C. Paris (Eds.), *Fatigue and Fracture mechanics*, ASTM STP 1360, ASTM, West Conshohocken, PA, 2000.
- [23] T.A. Phan, H. Oguchi, M. Hara, M. Shikida, H. Hida, T. Ando, K. Sato, H. Kuwano, Fe-B-Nd-Nb metallic glass thin films for microelectromechanical systems, *Appl. Phys. Lett.* 103 (18) (2013) 181901.
- [24] C.-L. Li, J.P. Chu, J.-W. Lee, Measuring notch toughness of thin film metallic glasses using focused ion beam-based microcantilever method: comparison with Ti and TiN crystalline films, *Mater. Sci. Eng. A* 698 (2017) 104–109.
- [25] D. Sorensen, E. Hintsala, J. Stevick, J. Pischlar, B. Li, D. Kiener, J.C. Myers, H. Jin, J. Liu, D. Stauffer, A.J. Ramirez, R.O. Ritchie, Intrinsic toughness of the bulk-metallic glass Vitreloy 105 measured using micro-cantilever beams, *Acta Mater.* 183 (2020) 242–248.
- [26] V. Schnabel, B.N. Jaya, M. Köhler, D. Music, C. Kirchlechner, G. Dehm, D. Raabe, J.M. Schneider, Electronic hybridisation implications for the damage-tolerance of thin film metallic glasses, *Sci. Rep.* 6 (2016) 36556.
- [27] P. Kontis, M. Köhler, S. Evertz, Y.T. Chen, V. Schnabel, R. Soler, J. Bednarick, C. Kirchlechner, G. Dehm, D. Raabe, J.M. Schneider, B. Gault, Nano-laminated thin film metallic glass design for outstanding mechanical properties, *Scr. Mater.* 155 (2018) 73–77.
- [28] G.P. Zhang, Y. Liu, B. Zhang, Effect of annealing close to T_g on notch fracture toughness of Pd-based thin-film metallic glass for MEMS applications, *Scr. Mater.* 54 (5) (2006) 897–901.
- [29] J. Wang, R. Li, N. Hua, T. Zhang, Co-based ternary bulk metallic glasses with ultrahigh strength and plasticity, *J. Mater. Res.* 26 (16) (2011) 2072–2079.
- [30] G. Dehm, B.N. Jaya, R. Raghavan, C. Kirchlechner, Overview on micro- and nanomechanical testing: new insights in interface plasticity and fracture at small length scales, *Acta Mater.* 142 (2018) 248–282.
- [31] C. Wang, Q.P. Cao, X.D. Wang, D.X. Zhang, U. Ramamurty, R.L. Narayan, J.Z. Jiang, Intermediate temperature brittleness in metallic glasses, *Adv. Mater.* 29 (2017) 1605537.
- [32] D. Raut, R.L. Narayan, P. Tandaiya, U. Ramamurty, Temperature-dependence of mode I fracture toughness of a bulk metallic glass, *Acta Mater.* 144 (2018) 325–336.
- [33] E. CommitteeE399–12e1 Standard Test Method For Linear-Elastic Plane-Strain Fracture Toughness K_{IC} of Metallic Materials, ASTM International, West Conshohocken, PA, 2012.
- [34] F. Iqbal, J. Ast, M. Göken, K. Durst, In situ micro-cantilever tests to study fracture properties of NiAl single crystals, *Acta Mater.* 60 (3) (2012) 1193–1200.
- [35] X.K. Xi, D.Q. Zhao, M.X. Pan, W.H. Wang, Y. Wu, J.J. Lewandowski, Fracture of brittle metallic glasses: brittleness or plasticity, *Phys. Rev. Lett.* 94 (2005) 125510.
- [36] I. Singh, R. Narasimhan, U. Ramamurty, Cavitation-induced fracture causes nanocorrugations in brittle metallic glasses, *Phys. Rev. Lett.* 117 (4) (2016).
- [37] R.L. Narayan, P. Tandaiya, R. Narasimhan, U. Ramamurty, Wallner lines, crack velocity and mechanisms of crack nucleation and growth in a brittle bulk metallic glass, *Acta Mater.* 80 (2014) 407–420.
- [38] R.L. Narayan, D. Raut, U. Ramamurty, A quantitative connection between shear band mediated plasticity and fracture initiation toughness of metallic glasses, *Acta Mater.* 150 (2018) 69–77.
- [39] T.L. Anderson, *Fracture Mechanics: Fundamentals and Applications*, 3rd ed., CRC Press, Boca Raton, 2005.
- [40] R.O. Ritchie, A.W. Thompson, On macroscopic and microscopic analyses for crack initiation and crack growth toughness in ductile alloys, *Metall. Trans. A* 16 (2) (1985) 233–248.
- [41] P. Tandaiya, R. Narasimhan, U. Ramamurty, On the mechanism and the length scales involved in the ductile fracture of a bulk metallic glass, *Acta Mater.* 61 (5) (2013) 1558–1570.
- [42] A. Bharathula, S.-W. Lee, W.J. Wright, K.M. Flores, Compression testing of metallic glass at small length scales: effects on deformation mode and stability, *Acta Mater.* 58 (17) (2010) 5789–5796.
- [43] R.O. Ritchie, The conflicts between strength and toughness, *Nat. Mater.* 10 (2011) 817–822.
- [44] J.J. Lewandowski, W.H. Wang, A.L. Greer, Intrinsic plasticity or brittleness of metallic glasses, *Philos. Mag. Lett.* 85 (2) (2005) 77–87.
- [45] J. Xu, U. Ramamurty, E. Ma, The fracture toughness of bulk metallic glasses, *JOM* 62 (4) (2010) 10–18.
- [46] R.T. Qu, H.S. Liu, Z.F. Zhang, In situ observation of bending stress-deflection response of metallic glass, *Mater. Sci. Eng. A* 582 (2013) 155–161.
- [47] W. Chen, H. Zhou, Z. Liu, J. Ketkaew, L. Shao, N. Li, P. Gong, W. Samela, H. Gao, J. Schroers, Test sample geometry for fracture toughness measurements of bulk metallic glasses, *Acta Mater.* 145 (2018) 477–487.
- [48] J.I. Bluhm, A model for the effect of thickness on fracture toughness, *ASTM Proc.* 61 (1961) 1324–1331.
- [49] S. Suresh, R.O. Ritchie, Propagation of short fatigue cracks, *Int. Met. Rev.* 29 (1984) 445–475.
- [50] H. Gao, B. Ji, I.L. Jäger, E. Arzt, P. Fratzl, Materials become insensitive to flaws at nanoscale: lessons from nature, *Proc. Natl. Acad. Sci. USA* 100 (10) (2003) 5597–5600.